

## Three-body model for $p$ -wave pion- $^{16}\text{O}$ scattering

K. A. Kabir, M. Silver,\* and N. Austern

*Department of Physics and Astronomy, University of Pittsburgh, Pittsburgh, Pennsylvania 15260*

(Received 13 September 1982)

A calculation of the elastic scattering of mesons from  $^{16}\text{O}$  is performed, using a modification of the first-order multiple scattering theory of Kerman, McManus, and Thaler, in which Pauli blocking effects are omitted from the  $\tau$  operator. The modified  $\tau$  operator is calculated in a three-body model, in which the struck nucleon is allowed to recoil in a Woods-Saxon nuclear shell model potential exerted by the remainder of the nucleus. The interaction between the meson and the struck nucleon is described by a separable potential. A set of coupled differential equations that describe the elastic and the excited channel wave functions is derived by approximating the shell model binding potential in the excited states of the nucleon as a potential for the meson-nucleon center of mass. This approximation is examined in detail. It is found that in the three-body model the bound states and the single particle resonances of the shell model potential alter the results significantly from those obtained in impulse approximation.

[ NUCLEAR REACTIONS  $^{16}\text{O}(\pi,\pi)$ , three-body model of  $\pi$ -nucleon interaction.  $\sigma_T(E)$  calculated. ]

### I. INTRODUCTION

This article continues the previous study of meson-nucleus elastic scattering by Silver and Austern<sup>1</sup> (SA), based on a three-body model of the underlying meson-nucleus  $\tau$  operator, in a first order multiple scattering theory. We now introduce a more realistic  $l=1$  meson-nucleon interaction, in place of the artificial resonant  $l=0$  interaction used previously. We also treat the spectrum of the excited single-particle orbitals more completely.

A multiple scattering theory of elastic scattering requires two sets of projection operators, one to select antisymmetric nuclear states, and one to select the ground state. These projectors can be introduced in various combinations. For example, the Kerman, McManus, Thaler<sup>2</sup> approach (KMT) develops an antisymmetrized multiple scattering formalism that is subsequently projected on the nuclear ground state. An alternative projected formalism<sup>3</sup> first isolates the role of the ground state and then develops a multiple scattering expansion. This alternative approach was applied in SA.

As it happens, the KMT approach and the projected approach are not only equivalent if both are developed exactly; it can be proved<sup>4,5</sup> that these approaches also give identical elastic scattering amplitudes to first order in multiple scattering theory. We therefore adopt the KMT approach for the present work, because the first-order KMT expres-

sions are not cluttered with ground state projection operators. The KMT  $\tau$  operator uses the entire spectrum of antisymmetric target nucleus eigenstates.

We develop a Schrödinger theory of meson scattering, in which the pion has a definite coordinate and retains its identity, and in which all particles interact by means of specified potentials. In our three-body model of the underlying  $\tau$  operator, practical calculation requires a kinematic approximation of the excited nucleon intermediate states,<sup>1,4,6</sup> as explained in Sec. II. This approximation emphasizes the center of mass coordinate of the pion and the nucleon, as if they formed a  $\Delta$  particle. The same approximation has been applied by Dedonder and Schmit,<sup>7</sup> by Garcilazo and Gibbs,<sup>8</sup> and in the interesting collective analysis in related "isobar doorway" studies by Hirata, Lenz, Koch, Yazaki, and Moniz<sup>9</sup> and Freedman, Henley, and Miller.<sup>10</sup> However, we retain standard shell model potentials in the excited states. Woods-Saxon potentials are used, to allow a reasonable evaluation of scattering in the nuclear surface region.

The three-body theory allows a quite accurate treatment of the recoil of each individual struck nucleon from which the meson scatters. However, the antisymmetrization in this theory is a little obscure. Although the emphasis on individual nucleons suggests calculation with Watson  $t_i$  operators instead of the antisymmetrized KMT  $\tau$  operator, or the corre-

sponding partially-antisymmetrized  $\tau_i$ , analyses of Pauli blocking disclose major differences between  $t_i$  and  $\tau_i$ . For example, blocking effects in the  $\tau_i$  operators strongly influence the results in the isobar doorway calculations.<sup>9-11</sup> On the other hand, the blocking analysis in that work proceeds by a calculation that is second order in  $t_i$ , to produce  $\tau_i$  operators that are used subsequently to derive a *first-order optical potential*. We recall that in one of the original discussions of blocking, Feshbach, Gal, and Hufner<sup>12</sup> found that if the KMT optical potential is calculated consistently to second order in  $t_i$ , using closure simplifications, then the second order blocking terms contained in  $\tau$  largely cancel against other terms in the optical potential that are of second order in  $\tau$ . In their work the surviving Pauli correlation effects are weak and can reasonably be disregarded. Similar arguments that Pauli blocking is weak are given by other authors.<sup>13</sup> On this evidence we adopt the opinion that Pauli effects are carried most consistently if the KMT optical potential is calculated in a (modified) first order, using Watson  $t_i$  operators in place of KMT  $\tau_i$  operators. Further analysis of this question could be interesting.

The basic kinematic approximation of the three-body model is considered in detail in Sec. IV, in an analysis of the "frame potential" of the three-body system. This approximation is seen to be more accurate than might be at first supposed.

Section V presents the main results of the calculation. It opens with a sketch of impulse approximation models, for comparison with our results. Differential cross sections and excitation functions for total cross sections then follow. Most of the new features of these cross sections seem to occur because the average excitation energies in the three-body model are much lower than in impulse approximation. A detailed analysis of the distribution of reaction strength with respect to excitation energy follows in Sec. VC. We then examine the radial behavior of the meson optical potential, and we find that it has a quite long range. Section VI is a brief summary.

## II. THE THREE-BODY MODEL

In this section the three-body model of the KMT elastic optical potential is formulated. Nonrelativistic expressions are given. Relativistic kinematics are inserted later when calculations are performed.

The total Hamiltonian of the  $\pi$ - $A$  system is

$$H = H_0 + V, \quad (1)$$

where

$$H_0 = K_\pi + H_T \quad (2)$$

and

$$V = \sum_i v_i. \quad (3)$$

In the above expressions  $K_\pi$  is the kinetic energy of the pion,  $H_T$  is the internal Hamiltonian of the nucleus,  $v_i$  is the two body interaction between the pion and the  $i$ th nucleon, and  $A$  is the total number of nucleons in the nucleus. The target nucleus is assumed to be at rest at the origin.

We use the coordinate  $\vec{s}$  to describe the pion and coordinates  $\vec{r}_1, \vec{r}_2, \dots, \vec{r}_A$  to describe the motion of the nucleons. We suppress the spin and isospin variables of the nucleons. In terms of these coordinates the antisymmetrized nuclear eigenfunctions are denoted by  $\Phi_\alpha(\vec{r}_1, \vec{r}_2, \dots, \vec{r}_A)$  with eigenvalues  $\mathcal{E}_\alpha$ , i.e.,

$$H_T \Phi_\alpha(r_1, r_2, \dots, r_A) = \mathcal{E}_\alpha \Phi_\alpha(r_1, r_2, \dots, r_A). \quad (4)$$

To describe the scattering we have to solve the Schrödinger equation

$$(E - H_0)\Psi = V\Psi \quad (5)$$

with appropriate boundary conditions. However, in the KMT procedure one introduces instead an auxiliary wave function  $\Psi'$  that satisfies

$$(E - H_0)\Psi' = (A - 1)\tau\Psi', \quad (6)$$

in terms of an antisymmetrized one-nucleon  $\tau$  operator for which

$$\tau = v + vG\tau, \quad (7)$$

with

$$G = \frac{\mathcal{A}}{E - H_0 + i\epsilon}. \quad (8)$$

Here  $\mathcal{A}$  is the antisymmetrization operator. The complete  $\Psi$  can be obtained from  $\Psi'$  by

$$\Psi = \Psi' + G\tau\Psi'. \quad (9)$$

The scattered amplitudes obtained from  $\Psi$  are  $A/(A - 1)$  times the amplitudes obtained from  $\Psi'$ .

The projection of  $\Psi'$  on the nuclear ground state is written as

$$P\Psi' = F'(\vec{s})\Phi_0(\vec{r}_1, \vec{r}_2, \dots, \vec{r}_A). \quad (10)$$

To first order in  $\tau$ , an optical equation for the meson wave function  $F'(\vec{s})$  is obtained from Eq. (6) in the form

$$(E - \mathcal{E}_0 - K_\pi)F'(\vec{s}) = (A - 1)(\Phi_0, \tau\Phi_0 F'). \quad (11)$$

Thus  $(A - 1)(\Phi_0, \tau\Phi_0)$  is the optical operator for  $F'(\vec{s})$ .

For an antisymmetric nuclear ground state it is convenient to replace  $\tau$  by

$$\tau = A^{-1} \sum_i \tau_i, \quad (12)$$

in terms of contributions from individual labeled nucleons, so that Eq. (11) can be rewritten as

$$(E - \mathcal{E}_0 - K_\pi) F'(\vec{s}) = \left[ \frac{A-1}{A} \right] \left[ \Phi_0, \sum_i \tau_i \Phi_0 F' \right]. \quad (13)$$

The relation to corresponding Watson  $t_i$  operators is given by<sup>12</sup>

$$\tau = A^{-1} \sum_i t_i \mathcal{A} + A^{-1} \sum_i t_i \frac{\mathcal{A} - 1}{E - H_0 + i\epsilon} \tau_i, \quad (14)$$

with

$$t_i \equiv v_i + v_i \frac{1}{E - H_0 + i\epsilon} t_i, \quad (15)$$

with no antisymmetrizers in (15). The second term in  $\tau$  in (14) corrects for Pauli-violating intermediate states in  $t_i$ . It was already explained in the Introduction that if we would extend the calculation of the optical potential to second order, then the second term of (14) would largely cancel against other second-order terms of similar structure. We therefore omit the second term of (14) and adopt the simple substitution

$$\tau \rightarrow A^{-1} \sum_i t_i \mathcal{A}, \quad (16)$$

to be used in (11) in the modified first-order optical potential.

The presence of the target Hamiltonian  $H_T$  in the propagator of (15) makes  $t_i$  a many-body operator. Following SA, Revai,<sup>6</sup> Tandy, Redish, and Bollé,<sup>4</sup> Garcilazo and Gibbs,<sup>8</sup> and the isobar doorway calcu-

lations<sup>9,10</sup> we reduce the many-body problem to a three-body problem by isolating the  $i$ th nucleon of the target and treating the rest of the nucleons as a passive core. We write the target Hamiltonian as

$$H_T = K_i + K_c + H_c + \omega_i, \quad (17)$$

where  $K_i$  is the kinetic energy of the  $i$ th nucleon,  $K_c$  is the kinetic energy of the center of mass of the core,  $H_c$  is the internal Hamiltonian of the core, and  $\omega_i = \sum_j v_{ij}$  is the interaction of the  $i$ th nucleon with the rest of the nucleus;  $\omega_i$  can give rise to many-body intermediate states since it involves the coordinates of all the nucleons. The three-body approximation consists of replacing  $\omega_i$  by the single particle potential  $U_i(r_i)$ . For simplicity, we neglect the recoil of the core, i.e., we set  $K_c = 0$ . This is a good approximation if the mass of the core is much larger than the mass of one nucleon plus a pion. The error due to this simplification is of the order of  $1/A$ . We now solve Eq. (15) for  $t_i$  in terms of  $v_i$  and insert the above approximations to obtain

$$t_i = v_i + v_i \frac{1}{E - H_c - K_\pi - K_i - U_i - v_i + i\epsilon} v_i. \quad (18)$$

Since  $H_c$  does not involve the coordinates of the pion or of the  $i$ th nucleon, it represents a simple shift of the total collision energy  $E$ . At this stage we have a three-body problem—the bodies being the incident pion, the  $i$ th nucleon, and the core. The interactions between these particles are  $V_{\pi i} = v_i$ ,  $V_{\pi c} = 0$ , and  $V_{ic} = U_i$ .

The optical potential in Eq. (11) has now been reduced to the expectation of a symmetric one-body operator for the nucleons. If the ground-state wave function  $\Phi_0$  for a closed-shell target nucleus is taken to be a Slater determinant of occupied single-particle orbitals, then the optical potential becomes a sum over these orbitals, and (11) becomes

$$[E - \mathcal{E}_0 - K_\pi] F'(\vec{s}) = \frac{A-1}{A} \sum_{\substack{n \\ \text{(occupied)}}} \left[ (\psi_n, v \psi_n F') + \left( \psi_n, v \frac{1}{E - \mathcal{E}_0 + \epsilon_n - K_\pi - K_N - U(r) - v + i\epsilon} v \psi_n F' \right) \right], \quad (19)$$

where  $\psi_n$  are single particle orbitals with energy  $\epsilon_n$ ,

$$[K_N + U(r)] \psi_n(\vec{r}) = \epsilon_n \psi_n(\vec{r}), \quad (20)$$

and

$$K_\pi = -(\hbar^2/2m_\pi) \nabla_{\vec{s}}^2$$

and

$$K_N = -(\hbar^2/2m_N) \nabla_{\vec{r}}^2$$

are the kinetic energy operators of the pion and the

nucleon, respectively. Equation (19) gives the wave function of the pion in the pion-nucleus center of mass frame. We need further approximations for a complete numerical solution of (19).

In solving Eq. (19) we use two sets of coordinates  $(\vec{r}, \vec{s})$  and  $(\vec{R}, \vec{\rho})$  to describe the motion of the pion and the nucleon;  $\vec{r}$  and  $\vec{s}$  are the coordinates of the nucleon and the pion relative to the  $\pi$ - $A$  center of mass,  $\vec{R}$  is the coordinate of the  $\pi N$  center of mass, and  $\vec{\rho}$  is the relative  $\pi N$  displacement. The transformations between these two sets of coordi-

nates are

$$\vec{R} = \bar{v}\vec{r} + v\vec{s}, \quad \vec{\rho} = \vec{s} - \vec{r} \quad (21a)$$

and

$$\vec{r} = \vec{R} - v\vec{\rho}, \quad \vec{s} = \vec{R} + \bar{v}\vec{\rho}, \quad (21b)$$

where

$$v = m_\pi / (m_\pi + m_N); \quad \bar{v} = 1 - v. \quad (21c)$$

The kinetic energy operator  $K_\pi + K_N$  separates in the two sets of coordinates,

$$\begin{aligned} K_\pi + K_N &= -\frac{\hbar^2}{2m_\pi} \nabla_{\vec{s}}^2 - \frac{\hbar^2}{2m_N} \nabla_{\vec{r}}^2 \\ &= -\frac{\hbar^2}{2\mu} \nabla_{\vec{\rho}}^2 - \frac{\hbar^2}{2M} \nabla_{\vec{R}}^2, \end{aligned} \quad (21d)$$

where

$$\mu = m_\pi m_N / (m_\pi + m_N)$$

is the  $\pi N$  reduced mass and  $M = m_\pi + m_N$  is the total mass of the pion and the nucleon.

We note that the binding potential of the nucleon  $U(r)$  in Eq. (19) is expressed in the coordinate set  $(\vec{r}, \vec{s})$ , and the  $\pi N$  interaction  $v$  is expressed in the coordinate set  $(\vec{R}, \vec{\rho})$ . To take full advantage of the short ranged nature of  $v(\rho)$  we evaluate the Green's function in the second term on the right-hand side of Eq. (19) in the  $(\vec{R}, \vec{\rho})$  coordinates. We then have to express the binding potential  $U(r)$  in terms of  $\vec{R}$  and  $\vec{\rho}$ . We write

$$U(r) = U(R) - [U(R) - U(r)]. \quad (22)$$

The term within the brackets is the error incurred in replacing  $r$  by  $R$  in the binding potential.

The Schrödinger equation (19) for  $F'(\vec{s})$  easily becomes a set of coupled equations. By use of Eq. (22)

these equations take the form

$$\begin{aligned} [E - \mathcal{E}_0 - K_\pi(\vec{s})]F'(\vec{s}) \\ = \frac{A-1}{A} \sum_n [(\psi_n, v\psi_n F') + (\psi_n, vG_n(\vec{R}, \vec{\rho}))] \end{aligned} \quad (23)$$

and

$$\begin{aligned} [E - \mathcal{E}_0 + \epsilon_n - K_{\vec{R}} - U(R) - K_{\vec{\rho}} - v]G_n(\vec{R}, \vec{\rho}) \\ = v\psi_n F' + [U(r) - U(R)]G_n(\vec{R}, \vec{\rho}), \end{aligned} \quad (24)$$

where

$$K_{\vec{R}} = -(\hbar^2/2M)\nabla_{\vec{R}}^2$$

and

$$K_{\vec{\rho}} = -(\hbar^2/2\mu)\nabla_{\vec{\rho}}^2.$$

The second term on the right-hand side of (24) arises because we transformed the binding potential  $U(r)$  to  $(\vec{R}, \vec{\rho})$  coordinates. Later in Sec. IV we shall show that this term, called the frame potential term, is small for important situations and can be neglected. We solve Eqs. (23) and (24) with the frame potential term set to zero, to get the elastic scattering wave function  $F'(\vec{s})$  of the pion, in the pion-nucleus center-of-mass frame.

### III. INPUTS TO THE OPTICAL POTENTIAL

The basic ingredient in the construction of the pion nucleus ( $\pi A$ ) optical potential is the pion nucleon ( $\pi N$ ) potential  $v$ . Because at medium energies the  $\pi N$  interaction is dominated by the 33 resonance in the relative  $l=1$  state, which tends to be separable in structure, it has been considered plausible to choose  $v$  to be an  $l=1$  separable interaction.<sup>14</sup> We choose the following form:

$$\langle \vec{\rho} | v | \vec{\rho}' \rangle = \frac{4\pi}{2l_0+1} v(\rho)v(\rho') \sum_{m_0} Y_{l_0 m_0}(\hat{\rho}) Y_{l_0 m_0}^*(\hat{\rho}') P_{j=3/2} P_{I=3/2}, \quad (25)$$

where  $l_0=1$ ;  $P_{j=3/2}$  is the projection operator on the  $\pi N$  state of total angular momentum  $j = \frac{3}{2}$ ;  $P_{I=3/2}$  is the projection operator on the  $\pi N$  state of isospin  $I = \frac{3}{2}$ ; and  $\vec{\rho}$  and  $\vec{\rho}'$  are the relative  $\pi N$  coordinates.

The  $t$  matrix in the  $\pi N$  center of mass is then

$$\langle \vec{\rho} | t(E) | \vec{\rho}' \rangle = \frac{4\pi}{2l_0+1} \frac{v(\rho)v(\rho')}{1 - I_{l_0}(q)} \sum_{m_0} Y_{l_0 m_0}(\hat{\rho}) Y_{l_0 m_0}^*(\hat{\rho}') P_{j=3/2} P_{I=3/2}, \quad (26)$$

where

$$I_{l_0}(q) = \frac{4\pi}{2l_0+1} \int_0^\infty d\rho \rho v(\rho) \int_0^\infty d\rho' g_{l_0}^{(+)}(q; \rho, \rho') \rho' v(\rho'), \quad (27)$$

with

$$g_{l_0}^{(+)}(q; \rho, \rho') = -iq \left[ \frac{2\mu}{\hbar^2} \right] \rho \rho' j_{l_0}(q\rho) h_{l_0}^{(1)}(q\rho') \quad (28)$$

as the outgoing radial Green's function;  $\mu$  is the reduced mass of the pion and the nucleon;

$$q = (2\mu E / \hbar^2)^{1/2}$$

is the wave number in the  $\pi N$  center of mass frame;  $j_{l_0}(q\rho)$  is the spherical Bessel function; and  $h_{l_0}^{(1)}(q\rho)$  is the spherical Hankel function,  $h_l^{(1)} = j_l + in_l$ , where  $n_l$  is the spherical Neumann function.

In momentum space the  $\pi N t$  matrix becomes

$$\begin{aligned} & \langle \vec{k} | t(E) | \vec{k}' \rangle \\ &= \frac{4\pi}{2l_0 + 1} \frac{\bar{v}_{l_0}(k) \bar{v}_{l_0}(k')}{1 - I_{l_0}(q)} \\ & \times \sum_{m_0} Y_{l_0 m_0}(\hat{k}) Y_{l_0 m_0}^*(\hat{k}') P_{j=3/2} P_{l=3/2}, \quad (29) \end{aligned}$$

where  $\bar{v}_{l_0}(k)$  is the spherical Bessel transform of  $v(\rho)$ ,

$$\bar{v}_{l_0}(k) = \left[ \frac{2}{\pi} \right]^{1/2} \int_0^\infty d\rho \rho^2 j_{l_0}(k\rho) v(\rho). \quad (30)$$

We choose a Yamaguchi form for  $v(\rho)$ ,

$$v(\rho) = v_0 e^{-\gamma \rho}. \quad (31)$$

In momentum space

$$\bar{v}_{l_0}(q) = 2 \left[ \frac{2}{\pi} \right]^{1/2} \frac{v_0 q}{(\gamma^2 + q^2)^2}. \quad (32)$$

The two parameters  $\gamma$  and  $v_0$  are then adjusted to fit the  $\pi N$  phase shifts  $\delta_{33}$  in the 33 channel. The parameters are found to be<sup>1,15</sup>

$$\gamma = 3.91 \text{ fm}^{-1}$$

and

$$v_0^2 = -6.26 \times 10^4 \text{ MeV/fm}^3,$$

where relativistic kinematics<sup>15,16</sup> is used to fit the phase shifts.

The binding potential,  $U(r)$ , of the nucleon is chosen to be a Woods-Saxon well,

$$U(r) = \frac{U_0}{1 + \exp \left[ \frac{r - R}{a} \right]}, \quad (33)$$

where the parameters are chosen to fit the energies of the occupied single particle orbitals of  $^{16}\text{O}$ . We find  $U_0 = -57.0$  MeV,  $R = r_0 A^{1/3}$  with  $r_0 = 1.25$  fm, and  $a = 0.5$  fm. The bound state energy levels in this potential are  $\epsilon_{1s} = -37.79$  MeV,  $\epsilon_{1p} = -22.15$  MeV,  $\epsilon_{1d} = -5.97$  MeV, and  $\epsilon_{2s} = -5.28$  MeV. In the independent particle model of  $^{16}\text{O}$  the 1s and 1p

orbitals are completely filled and the root mean square (rms) radius is found to be 2.4 fm.

#### IV. CALCULATIONAL PROCEDURES

In subsection A of this section we outline details of the partial wave analysis of the coupled equations (23) and (24) and we comment about a factorization approximation used in certain multiple integrals. In subsection B we investigate the importance of the frame potential [the second term on the right-hand side of Eq. (24)]. The final expressions used in numerical calculations are summarized in subsection C.

##### A. Partial wave analysis

To solve the coupled equations (23) and (24) we introduce partial wave expansions (the prime on  $F'$  is omitted)

$$F(\vec{s}) = \sum_{J, \mathcal{M}} \frac{F^J(s)}{s} Y_{J, \mathcal{M}}(\hat{s}) \quad (34)$$

and

$$\begin{aligned} G_{aL_0 M_0}(\vec{R}, \vec{\rho}) &= \sum_{J, \mathcal{M}} \sum_{\epsilon L_1 L_1} \bar{\mathcal{Y}}_{\epsilon L_1 L_1}^{J, \mathcal{M}, L_0 M_0}(\vec{R}, \hat{\rho}) \\ & \times \frac{G_{a\epsilon}^J(L_0 L_1 L_1, \rho)}{\rho}, \quad (35) \end{aligned}$$

where

$$\begin{aligned} \bar{\mathcal{Y}}_{\epsilon L_1 L_1}^{J, \mathcal{M}, L_0 M_0}(\vec{R}, \vec{\rho}) &= \sum_{M_1 M m} \langle L_0 L_1 M_0 M_1 | LM \rangle \\ & \times \langle LIMm | J, \mathcal{M} \rangle \\ & \times \bar{\psi}_{\epsilon L_1}(R) Y_{L_1 M_1}(\hat{R}) Y_{lm}(\hat{\rho}). \quad (36) \end{aligned}$$

We use the label  $n \equiv \{a, L_0, M_0\}$  in (35) for the occupied single particle orbitals of  $^{16}\text{O}$ , where  $L_0$  and  $M_0$  are the orbital angular momentum and its projection, respectively, and  $a = \{m_s, m_\tau\}$  denotes the spin and isospin of the nucleon. The excited orbitals  $\bar{\psi}_{\epsilon L_1}(R) Y_{L_1 M_1}(\hat{R})$  in Eq. (36) are eigenfunctions of the pion-nucleon center-of-mass Hamiltonian  $K_R + U(R)$ , with energy  $\epsilon$  and angular momentum  $L_1$ . We note that  $L_0$  and  $L_1$  couple to  $L$ , the angular momentum transfer to the nucleon. The relative pion-nucleon angular momentum  $l$  couples with  $L$  to give  $J$ , which is both the incident angular momentum of the pion and the total angular momentum of the system. The sum over  $\epsilon$  in (35) runs through

discrete and continuous values.

We now use the orthogonality properties of Eqs. (34)–(36) and the explicit form of  $v$  given in Eq. (25) to obtain coupled equations for the radial wave

functions  $F^J(s)$  and  $G_{a\epsilon}^J(L_0L_1Ll;\rho)$ . However, the frame potential is omitted from the equations for  $G_{a\epsilon}^J$ , in anticipation of the discussion in Sec. IV B. Thus the coupled equations we treat are

$$[T_\pi - t_J(s)]F^J(s) = \frac{A-1}{A} \frac{4\pi}{2l_0+1} s \sum_{aL_0} \left[ W_{aL_0}^J F^J(s)/s + \sum_{\epsilon L_1 L} V_{a\epsilon}^J(L_0L_1Ll_0, s) A_{a\epsilon}^J(L_0L_1Ll_0) \right] \quad (37a)$$

and

$$[T_\pi + \epsilon_{aL_0} - \epsilon - t_l(\rho)]G_{a\epsilon}^J(L_0L_1Ll, \rho) = \delta_{ll_0} \frac{4\pi}{2l_0+1} \rho v(\rho) [B_{a\epsilon}^J(L_0L_1Ll) + A_{a\epsilon}^J(L_0L_1Ll)], \quad (37b)$$

where  $t_J(s)$  and  $t_l(\rho)$  are partial-wave kinetic energy operators, and

$$A_{a\epsilon}^J(L_0L_1Ll) = \int_0^\infty d\rho \rho v(\rho) G_{a\epsilon}^J(L_0L_1Ll, \rho), \quad (38a)$$

$$B_{a\epsilon}^J(L_0L_1Ll_0) = \int d\vec{R} \int d\vec{\rho} \sum_{\substack{M_0 M_1 \\ M m_0}} \bar{\psi}_{\epsilon L_1}^*(R) Y_{L_1 M_1}^*(\hat{R}) Y_{l_0 m_0}(\hat{\rho}) v(\rho) \\ \times \psi_{aL_0}(|\vec{R} - \nu\vec{\rho}|) Y_{L_0 M_0}^*(\hat{n}_{\vec{R} - \nu\vec{\rho}}) Y_{J, \mathcal{M}}(\hat{n}_{\vec{R} + \bar{\nu}\vec{\rho}}) \frac{F^J(|\vec{R} + \bar{\nu}\vec{\rho}|)}{|\vec{R} + \bar{\nu}\vec{\rho}|} \\ \times \langle L_0 L_1 M_0 M_1 | LM \rangle \langle Ll_0 M m_0 | J \mathcal{M} \rangle, \quad (38b)$$

$$V_{a\epsilon}^J(L_0L_1Ll_0, s) = \int d\vec{\rho} \int d\hat{s} \sum_{\substack{M_0 M_1 \\ M m_0}} Y_{J, \mathcal{M}}^*(\hat{s}) \psi_{aL_0}(|\vec{s} - \vec{\rho}|) Y_{L_0 M_0}(\hat{n}_{\vec{s} - \vec{\rho}}) v(\rho) \\ \times Y_{l_0 m_0}(\hat{\rho}) \bar{\psi}_{\epsilon L_1}(|\vec{s} - \bar{\nu}\vec{\rho}|) Y_{L_1 M_1}(\hat{n}_{\vec{s} - \bar{\nu}\vec{\rho}}) \\ \times \langle L_0 L_1 M_0 M_1 | LM \rangle \langle Ll_0 M m_0 | J \mathcal{M} \rangle, \quad (38c)$$

and

$$W_{aL_0}^J \frac{F^J(s)}{s} = \sum_{M_0 m_0} \int d\vec{\rho} \int d\hat{s} Y_{J, \mathcal{M}}^*(\hat{s}) \psi_{aL_0}(|\vec{s} - \vec{\rho}|) Y_{L_0 M_0}^*(\hat{n}_{\vec{s} - \vec{\rho}}) \\ \times v(\rho) Y_{l_0 m_0}(\hat{\rho}) \int d\vec{\rho}' Y_{l_0 m_0}^*(\hat{\rho}') v(\rho') \psi_{aL_0}(|\vec{s} - \bar{\nu}\vec{\rho}' - \nu\vec{\rho}|) Y_{L_0 M_0}(\hat{n}_{\vec{s} - \bar{\nu}\vec{\rho}' - \nu\vec{\rho}}) \\ \times \frac{F^J(|\vec{s} - \bar{\nu}\vec{\rho}' + \bar{\nu}\vec{\rho}|)}{|\vec{s} - \bar{\nu}\vec{\rho}' + \bar{\nu}\vec{\rho}|} Y_{J, \mathcal{M}}(\hat{n}_{\vec{s} - \bar{\nu}\vec{\rho}' + \bar{\nu}\vec{\rho}}). \quad (38d)$$

Here, for example,  $\hat{n}_{\vec{R} - \nu\vec{\rho}}$  is defined as a unit vector in the  $\vec{R} - \nu\vec{\rho}$  direction.

Equation (37b) is easily solved in closed form. We substitute this solution in (38a) to obtain an expression for  $A_{a\epsilon}^J$  in terms of  $B_{a\epsilon}^J$ , which in turn is substituted in Eq. (37a). The sequence of expressions obtained in this procedure is

$$A_{a\epsilon}^J(L_0L_1Ll_0) = \mathcal{R}(q) B_{a\epsilon}^J(L_0L_1Ll_0) \quad (39)$$

with

$$\mathcal{R}(q) = \frac{I_{l_0}(q)}{1 - I_{l_0}(q)} \quad (40)$$

and

$$q = [(2\mu/\hbar^2)(T_\pi + \epsilon_{aL_0} - \epsilon)]^{1/2}. \quad (41)$$

Here  $I_{l_0}(q)$  already appears in Eq. (27) in the separable-potential discussion of pion-nucleon scattering. The final substitution of Eq. (39) in (37a) gives

$$[T_\pi - t_J(s)]F^J(s) = \frac{A-1}{A} \frac{4\pi}{2l_0+1} s \sum_{aL_0} \left[ W_{aL_0}^J F^J(s)/s + \sum_{\epsilon L_1 L} V_{a\epsilon}^J(L_0 L_1 L l_0, s) \mathcal{R}(q) B_{a\epsilon}^J(L_0 L_1 L l_0) \right], \quad (42)$$

an optical model equation for the elastic scattering wave function of the pion in the  $\pi$ - $A$  center of mass frame. The function  $\mathcal{R}(q)$  introduces resonance effects in the optical potential.

We do not consider the spin and isospin variables of the nucleon explicitly. Since the  $\pi N$  potential  $v$  is chosen to be confined in the 33 channel [see Eq. (25)], and the expectation values of both the projection operators  $P_{j=3/2}$  and  $P_{I=3/2}$  are  $\frac{4}{3}$  for a closed shell nucleus, the sum over the spin and isospin variables indicated by the label  $a$  in (42) is replaced by a multiplicative factor of  $\frac{16}{9}$ .

The expressions for  $W_{aL_0}^J$ ,  $V_{a\epsilon}^J$ , and  $B_{a\epsilon}^J$  are difficult to generate. Therefore suitable approximations have to be made for them before one attempts to solve for  $F^J(s)$ . These approximations are discussed in detail in Ref. 5. They are extensions of the fac-

torization method introduced in SA, whereby the integrations over the short ranged functions  $v(\rho)$  are performed analytically by factoring the  $\vec{\rho}$  dependence in Eqs. (38b)–(38d), as if the wave functions were plane waves. The factorization approximation can be interpreted as a partial transformation to momentum space for the purpose of the  $\vec{\rho}$  integrations. If the entire calculation were formulated in momentum space this approximation would not be needed.

### B. Frame potential

In Sec. IV A we neglected the term involving  $U(r) - U(R)$  in the equation for  $G_{a\epsilon}^J(L_0 L_1 L l, \rho)$ . If we now restore this term, Eq. (37b) takes the extended form

$$[T_\pi + \epsilon_0 - \epsilon - t_i(\rho)] G_{\epsilon L l}^J(\rho) = \delta_{l1} \frac{4\pi}{3} \rho v(\rho) (1 + \mathcal{R}(q)) B_{\epsilon L l}^J + \sum_{\epsilon' L' l'} \int d\vec{R} \int d\hat{\rho} \mathcal{T}_{\epsilon L l}^{J \mathcal{M}}(\vec{R}, \hat{\rho}) [U(r) - U(R)] \mathcal{T}_{\epsilon' L' l'}^{J \mathcal{M}}(\vec{R}, \hat{\rho}) G_{\epsilon' L' l'}^J(\rho). \quad (43)$$

For simplicity of discussion we have specialized to the case  $L_0 = M_0 = 0$ ,  $l_0 = 1$ . For this case, the angular momentum functions in (43) are

$$\begin{aligned} \mathcal{T}_{\epsilon L l}^{J \mathcal{M}}(\vec{R}, \hat{\rho}) &= \sum_{Mm} \langle LIMm | J \mathcal{M} \rangle \\ &\quad \times \bar{\psi}_{\epsilon L}(R) Y_{LM}(\hat{R}) Y_{lm}(\hat{\rho}) \\ &\equiv \{ \bar{\psi}_{\epsilon L}(\vec{R}), Y_l(\hat{\rho}) \}_{J \mathcal{M}}. \end{aligned} \quad (44)$$

$$P_F(E, \epsilon, J, L, l, \rho) = [G_{\epsilon L l}^J(\rho)]^{-1} \sum_{L' l'} \int d\epsilon' \int d\vec{R} \int d\hat{\rho} \mathcal{T}_{\epsilon L l}^{J \mathcal{M}}(\vec{R}, \hat{\rho}) [U(r) - U(R)] \mathcal{T}_{\epsilon' L' l'}^{J \mathcal{M}}(\vec{R}, \hat{\rho}) G_{\epsilon' L' l'}^J(\rho). \quad (45)$$

The dependence of  $P_F$  on the total energy  $E = T_\pi + \mathcal{E}_0$  comes from  $G_{\epsilon' L' l'}^J(\rho)$  in the numerator and from  $G_{\epsilon L l}^J(\rho)$  in the denominator of Eq. (45).

Although the difference potential

$$U(r) - U(R) = U(|\vec{R} - v\vec{\rho}|) - U(R)$$

becomes zero as  $\rho \rightarrow 0$ , it remains finite for large  $\rho$ . But as we shall see, the energy averaging indicated in Eq. (45) makes the entire frame potential go to zero for large  $\rho$ . Since it is also a smooth function for all  $\rho$ , the  $P_F$  tends not to affect the outgoing

The second term on the right-hand side of (43) is the correction that arises from transforming  $U(r)$  to  $(\vec{R}, \vec{\rho})$  coordinates. To facilitate discussion we define an equivalent potential obtained by dividing this term by  $G_{\epsilon L l}^J(\rho)$ . We call this equivalent potential the frame potential,  $P_F$ .

boundary condition imposed on  $G_{\epsilon L l}^J(\rho)$ . It is a great simplification to drop the  $P_F$  term from Eq. (43), as is done in the main part of this work.

We begin our analysis of the  $P_F$  by expanding  $U(r) - U(R)$  in multipoles:

$$U(r) - U(R) = 4\pi \sum_{\lambda\mu} g_\lambda(R, \rho) Y_{\lambda\mu}^*(\hat{R}) Y_{\lambda\mu}(\hat{\rho}). \quad (46)$$

By inversion

$$g_\lambda(R, \rho) = \frac{1}{2} \int_{-1}^{+1} d(\hat{R} \cdot \hat{\rho}) [U(r) - U(R)] P_\lambda(\hat{R} \cdot \hat{\rho}). \quad (47)$$

To obtain numerical estimates of the  $P_F$  we now assume a Gaussian form for the binding potential, i.e.,

$$U(R) = U_0 e^{-\alpha^2 R^2},$$

with  $U_0 = -50.0$  MeV and  $\alpha = \frac{1}{2}$  fm. This poten-

tial has an  $s$  wave bound state with energy  $\epsilon = -14.1$  MeV. Then from (47) we get

$$g_\lambda(R, \rho) = U(R) \left[ i^\lambda \frac{U(\nu\rho)}{U_0} j_\lambda(-2i\alpha^2\nu\rho R) - \delta_{\lambda 0} \right], \quad (48)$$

where  $j_\lambda$  is the spherical Bessel function of order  $\lambda$ . Substituting (46) in (45) we get

$$P_F(E, \epsilon, J, L, l=1, \rho) = [G_{\epsilon L 1}^J(\rho)]^{-1} \times 4\pi \sum_{\lambda\mu} \sum_{L'L'} \int d\epsilon' d\vec{R} d\hat{\rho} \overline{\mathcal{Y}}_{\epsilon L 1}^{*J\lambda}(\vec{R}, \hat{\rho}) g_\lambda(R, \rho) Y_{\lambda\mu}^*(\hat{R}) Y_{\lambda\mu}^*(\hat{\rho}) \overline{\mathcal{Y}}_{\epsilon' L' 1}^{J\lambda}(\vec{R}, \hat{\rho}) G_{\epsilon' L' 1}^J(\rho). \quad (49)$$

From (49) and (48) we see that the higher order multipole terms in the  $P_F$  are small. For example, the quadrupole ( $\lambda=2$ ) term connects  $L=0$  with  $L'=2$ , hence the factor  $\overline{\psi}_{\epsilon L}^*(R) \overline{\psi}_{\epsilon' L'}(R)$  in the  $R$  integral is small, because centrifugal repulsion suppresses  $\overline{\psi}_{\epsilon L'=2}(R)$  at small  $R$ , where  $U(R)$  is appreciable. This effect becomes more pronounced as the multipole order increases. Furthermore, we see from (48) that in the important region  $R \ll 1/\alpha$  and  $\nu\rho \ll 1/\alpha$

$$g_\lambda(R, \rho) \underset{2\alpha^2\nu\rho R \ll \lambda}{\sim} U(R) \left[ i^\lambda \frac{U(\nu\rho)}{U_0} \frac{(-2i\alpha^2\nu\rho R)^\lambda}{(2\lambda+1)!!} - \delta_{\lambda 0} \right]. \quad (50)$$

Therefore, except for  $\lambda=0$ , all other  $g_\lambda(R, \rho)$  are reduced within the range of  $U(R)$ , this reduction being more pronounced as  $\lambda$  increases. Thus for large  $\lambda$ ,  $g_\lambda(R, \rho)$  and  $\overline{\psi}_{\epsilon L}^*(R) \overline{\psi}_{\epsilon' L'}(R)$  in the  $R$  integral of the  $P_F$  [Eq. (49)] are small inside the range of  $U(R)$ , making this integral and hence the frame potential small. These remarks resemble the arguments of Garcilazo and Gibbs,<sup>8</sup> who discarded the frame potential as an effect of order  $\mu/M$ .

We therefore expect the monopole term in the  $P_F$  to be dominant, with perhaps the dipole term next in importance. We can give a perturbative argument to show that even the dipole term is smaller than the monopole term: Equation (43) for  $G_{\epsilon L 1}^J(\rho)$  includes as its source terms both the strong  $\pi N$  potential  $v$  and the frame potential. The dipole term ( $\lambda=1$ ) of the frame potential couples  $G_{\epsilon L 1}^J(\rho)$  with  $G_{\epsilon' L' 1}^J(\rho)$  and  $G_{\epsilon' L' 2}^J(\rho)$ . However, the source terms in the differential equations for  $G_{\epsilon' L' 1}^J(\rho)$  and  $G_{\epsilon' L' 2}^J(\rho)$  involve only the frame potential. Therefore, the effect of the dipole term is in second order. On the other hand, the monopole term ( $\lambda=0$ ) of the frame potential couples  $G_{\epsilon L 1}^J(\rho)$  with  $G_{\epsilon' L' 1}^J(\rho)$ , and so the effect of the monopole term is in first order. The monopole frame potential, therefore, is expected to be the only strong term.

In what follows, we shall consider only the monopole frame potential,  $P_{\text{MPF}}$ . With  $\lambda=0$  in (49) we have

$$P_{\text{MPF}}(E, \epsilon, J, L, l=1, \rho) = [G_{\epsilon L 1}^J(\rho)]^{-1} \int d\epsilon' \int_0^\infty R^2 dR \overline{\psi}_{\epsilon L}^*(R) g_0(R, \rho) \overline{\psi}_{\epsilon' L}(R) G_{\epsilon' L 1}^J(\rho). \quad (51)$$

Now from (48)

$$g_0(R, \rho) = -f(R, \rho) U(R), \quad (52)$$

where

$$f(R, \rho) = 1 - \frac{U(\nu\rho)}{U_0} \frac{\sinh 2\alpha^2\nu\rho R}{2\alpha^2\nu\rho R}. \quad (53)$$

To simplify calculations of the  $P_{\text{MPF}}$  and to verify that its effects are small, we approximate  $g_0(R, \rho)$  as

$$g_0(R, \rho) \approx -C(\nu\rho) U(R), \quad (54)$$

where

$$C(\nu\rho) = 1 - \frac{U(\nu\rho)}{U_0}. \quad (55)$$

Because this simple approximation overestimates<sup>5</sup>  $g_0(R, \rho)$ , it does not prejudice our eventual conclusion that the  $P_{\text{MPF}}$  can be neglected. Indeed, Eq. (54) is of reasonable accuracy in the most interesting ranges of  $R$  and  $\rho$ . With the approximate expression (54) for  $g_0(R, \rho)$  inserted in (51) the monopole frame potential becomes

$$P_{\text{MPF}}(E, \epsilon, J, L, l=1, \rho) = [G_{\epsilon L 1}^J(\rho)]^{-1} (-C(\nu\rho)) \int d\epsilon' \int_0^\infty R^2 dR \bar{\psi}_{\epsilon L}(R) U(R) \bar{\psi}_{\epsilon' L}(R) G_{\epsilon' L 1}^J(\rho). \quad (56)$$

It is helpful to define an overlap function

$$D_{\epsilon L}(k, k') \equiv -\frac{\hbar^2 k'}{M} \int_0^\infty dR R^2 \bar{\psi}_{\epsilon L}(R) U(R) \bar{\psi}_{\epsilon' L}(R), \quad (57)$$

so that

$$P_{\text{MPF}}(E, \epsilon, J, L, l=1, \rho) = [G_{\epsilon L 1}^J(\rho)]^{-1} C(\nu\rho) \int_0^\infty dk' D_{\epsilon L}(k, k') G_{\epsilon' L 1}^J(\rho). \quad (58)$$

The nucleonlike wave functions  $\bar{\psi}_{\epsilon L}(R)$  in (57) are real and are normalized so that

$$\bar{\psi}_{\epsilon L}(R) \underset{R \rightarrow \infty}{\sim} \frac{1}{R} \left[ \frac{2M}{\pi \hbar^2 k} \right]^{1/2} \sin(kR - L\pi/2 + \delta_L). \quad (59)$$

Hence  $D_{\epsilon L}$  has the dimensions energy  $\times$  length. For convenience the signs of  $\bar{\psi}_{\epsilon L}(R)$  and  $\bar{\psi}_{\epsilon' L}(R)$  are adjusted so that  $D_{\epsilon L}(k, k')$  is a positive function for all  $k$  and  $k'$ . This does not affect the overall expression for  $P_{\text{MPF}}$  since  $\bar{\psi}_{\epsilon L}(R)$  also occurs in  $G_{\epsilon L 1}^J(\rho)$ . Now  $D_{\epsilon L}(k, k')$  can be easily calculated from the numerically obtained functions  $\bar{\psi}_{\epsilon L}(R)$ . Figure 1 shows plots of exact  $D_{\epsilon L}(k, k')$  for  $L=0$  and  $\epsilon=0.01, 4.5, 19.9, 49.1,$  and  $99.7$  MeV. Figures 2 and 3 show  $D_{\epsilon L}(k, k')$  for  $L=1$  and  $L=2$ , respectively.

For  $L=1$  (Fig. 2) the overlaps  $D_{\epsilon L}(k, k')$  are considerably larger at small  $k'$  and  $\epsilon$  than the corresponding overlaps for  $L=0$  and  $L=2$ . Also there is a peak in  $D_{\epsilon L=1}(k, k')$  at  $k \approx 0.2$  fm, the peak being more pronounced for smaller  $\epsilon$ . This is due to a resonance in the nucleonlike wave functions  $\bar{\psi}_{\epsilon L=1}(R)$ , corresponding to a barely unbound  $p$  state at  $k=0.2$  fm.

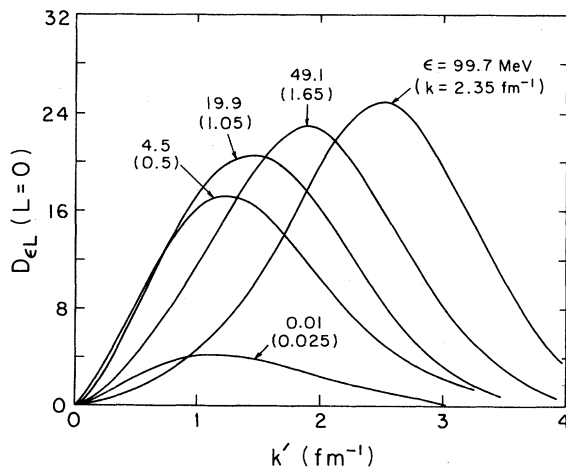


FIG. 1. Exact  $D_{\epsilon L}(k, k')$  for  $L=0$  and for  $\epsilon=0.01, 4.5, 19.9, 49.1,$  and  $99.7$  MeV obtained from Eq. (57). Note that  $\epsilon = \hbar^2 k^2 / 2M$ , where  $M$  is the mass of the pion plus the mass of the nucleon.  $D_{\epsilon L}(k, k')$  goes into the calculation of the  $P_{\text{MPF}}$  [Eq. (58)].

We now turn to the energy integral (i.e., the  $k'$  integral) in expression (58) for the  $P_{\text{MPF}}$ . In this integral we need the relative wave function  $G_{\epsilon L 1}^J(\rho)$ . In first approximation this wave function is the solution of (43) with the frame potential set to zero

$$G_{\epsilon L 1}^J(\rho) \approx \frac{4\pi}{3} [1 + \mathcal{P}(q')] B_{\epsilon L 1}^J \times \int_0^\infty d\rho' g_1^{(+)}(q'; \rho, \rho') \rho' v(\rho'). \quad (60)$$

The integral in Eq. (60) simplifies because  $v(\rho')$  has short range, and because the  $P_{\text{MPF}}$  primarily requires  $G_{\epsilon L 1}^J(\rho)$  at large  $\rho$ . We also obtain convenient expressions for  $B_{\epsilon L 1}^J$  from the factorization approximation (Sec. IV A). Under these approximations the  $k'$  integral in Eq. (58) is easily evaluated numerically and the  $P_{\text{MPF}}$  is evaluated. It is interesting that the  $P_{\text{MPF}}$  is independent of  $J$ , since the  $J$  dependence of  $G_{\epsilon L 1}^J$  only appears in a coefficient, and this cancels when division is performed.

Figure 4 shows the  $L=0$   $P_{\text{MPF}}$  for the typical incident energy  $E=100$  MeV, for various values of

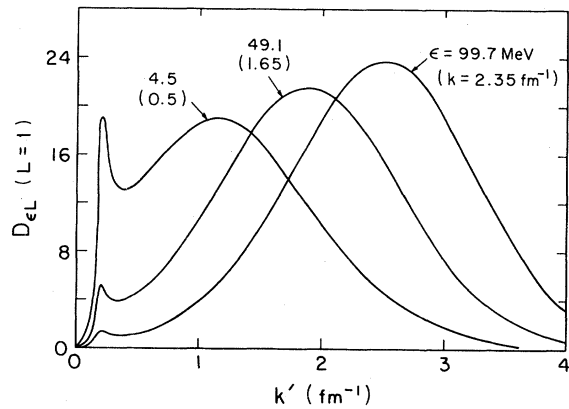


FIG. 2. Exact  $D_{\epsilon L}(k, k')$  for  $L=1$  and for  $\epsilon=4.5, 49.1,$  and  $99.7$  MeV.

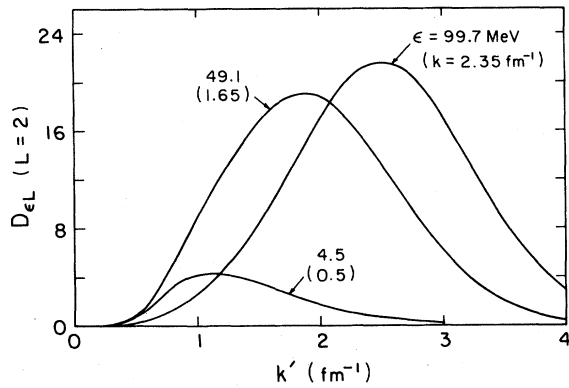


FIG. 3. Exact  $D_{eL}(k, k')$  for  $L=2$  and for  $\epsilon=4.5$ , 49.1, and 99.7 MeV.

nucleon excitation energy  $\epsilon$ . Figures 5 and 6 show the  $L=1$   $P_{\text{MPF}}$  for  $E=100$  and 280 MeV, respectively. The  $P_{\text{MPF}}$  for higher  $L$  values are similar.<sup>5</sup>

A general observation from these calculations is that in the important range of excitations (see Sec. V)  $\epsilon \ll E$ , the  $P_{\text{MPF}}$  is very weak compared to  $v(\rho)$ ; moreover, although it extends to long range it tends to be very smooth. Even at large  $\epsilon$  the oscillations of the  $P_{\text{MPF}}$  are slow. Under these circumstances the  $P_{\text{MPF}}$  should not have much influence on the solutions of Eq. (43) in the important region of small  $\rho$  required for the construction of the optical potential.

Two effects reduce the magnitude of the  $P_{\text{MPF}}$  at low  $\epsilon$ . First is that the  $D_{eL}(k, k')$  themselves tend to be small at small  $k'$ , because of poor penetration of the  $\bar{\psi}_{eL}$  wave functions into the region  $U(R) \neq 0$ . The weak  $L=1$  resonance at low  $k'$  does not modify this very much. Probably of greater importance is that the effect of  $U(R)$  in the function  $D_{eL}(k, k')$  extends over a large range of  $k'$  values. Only a small portion of this range has much overlap with the

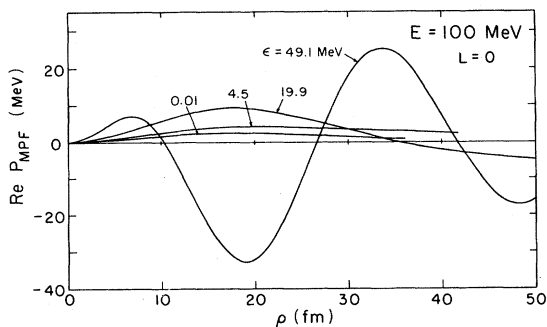


FIG. 4. Real part of the  $P_{\text{MPF}}$  for  $L=0$ ,  $E=100$  MeV and for  $\epsilon=0.01$ , 4.5, 19.9, and 49.1 MeV.

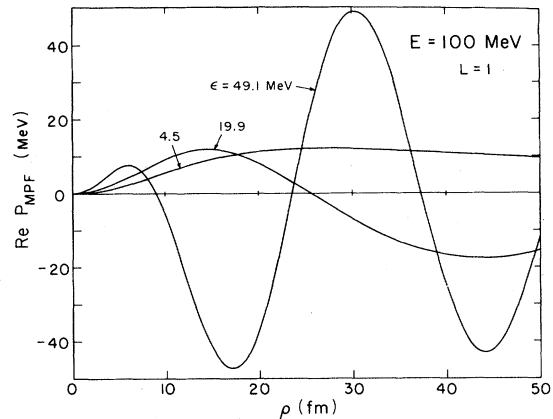


FIG. 5. Real part of the  $P_{\text{MPF}}$  for  $L=1$ ,  $E=100$  MeV and for  $\epsilon=4.5$ , 19.9, and 49.1 MeV.

function  $B_{e'L_1}^J$  in Eq. (60), which expresses the coupling of  $G_{e'L_1}^J(\rho)$  to the elastic channel. (At all bombarding energies  $B_{e'L_1}^J$  is concentrated at low excitations, with a narrow peak at  $k' \approx 0.4 \text{ fm}^{-1}$ .)

Probably the principal reason why the  $P_{\text{MPF}}$  at low  $\epsilon$  is a smooth function of  $\rho$  is that  $B_{e'L_1}^J$  is localized at low  $e'$ , therefore the oscillations of the denominator in Eq. (58) tend to cancel those of the numerator. This effect is lost as  $\epsilon$  becomes larger, and we then obtain the oscillatory  $P_{\text{MPF}}$  seen at large  $\epsilon$  in Figs. 4–6. Because  $G_{e'L_1}^J$  in the denominator is a rapidly decreasing function of  $\epsilon$ , the  $P_{\text{MPF}}$  is not only oscillatory at large  $\epsilon$ , it has a large magnitude. We conclude that at large  $\epsilon$  it is not satisfactory to omit the  $P_{\text{MPF}}$  from Eq. (43). Fortunately excitations to large  $\epsilon$  are not important in the overall calculation of the meson optical potential (Sec. V).

Another effect that tends to reduce the oscillations of the  $P_{\text{MPF}}$  at large  $\rho$  is the averaging over  $\epsilon'$  values in the numerator of Eq. (58). This averaging reduces the strength of the  $P_{\text{MPF}}$  at large  $\rho$ , with the result that although this potential has long range, its

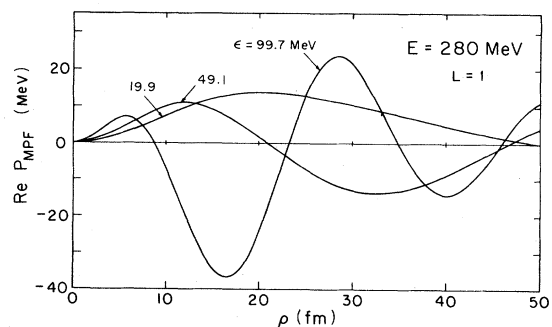


FIG. 6. Real part of the  $P_{\text{MPF}}$  for  $L=1$ ,  $E=280$  MeV and for  $\epsilon=19.9$ , 49.1, and 99.7 MeV.

range remains finite. Rough analytic approximations provide reasonable estimates of this range.<sup>5</sup> Mild oscillations of such a finite-ranged function are of little consequence.

In summary, at low  $\epsilon$  the  $P_{\text{MPF}}$  can be omitted from Eq. (43), because it is too weak and too long ranged to affect the equation in the region  $v(\rho) \neq 0$  and it is too smooth to affect the outgoing boundary condition. Although the  $P_{\text{MPF}}$  is not negligible at high  $\epsilon$ , the intermediate states  $\psi_{\epsilon L}$  at high  $\epsilon$  are not physically important; therefore its omission is not damaging.

### C. Optical equation

We return to the optical model equation (42) for the KMT auxiliary radial wave function  $F^J(s)$ . This

$$\int V_{\text{opt}}^J(s, s') F^J(s') ds' = \frac{4\pi}{2l_0 + 1} s \sum_{aL_0} \left[ W_{aL_0}^J F^J(s)/s + \sum_{\epsilon L_1 L} V_{a\epsilon}^J(L_0 L_1 L l_0, s) \mathcal{R}(q) B_{a\epsilon}^J(L_0 L_1 L l) \right]. \quad (63)$$

The quantities  $W_{aL_0}^J$ ,  $V_{a\epsilon}^J$ , and  $B_{a\epsilon}^J$  are derived<sup>5</sup> by the factorization approximation referred to in Sec. IV A. We note that our optical potential (63) is independent of the spin and isospin variables of the nucleons. Therefore the sum over  $a \equiv \{m_s, m_\tau\}$  in (63) is replaced by a multiplicative factor  $\frac{16}{9}$  as explained in Sec. IV A. We solve the Schrödinger equation by expanding  $F^J(s)$  in a suitable set of basis states.<sup>5</sup>

## V. RESULTS AND DISCUSSION

Using the optical potential developed in Secs. II–IV, we solve the Schrödinger equation (61) for the elastic scattering of pions from  $^{16}\text{O}$ . It should be noted that we have included only the  $p$  wave  $\pi N$  in-

equation omits frame potential effects. If relativistic kinematical corrections for the pion projectile are now inserted<sup>15,16</sup> the optical equation becomes

$$\left[ \frac{d^2}{ds^2} + k_0^2 - \frac{J(J+1)}{s^2} \right] F^J(s) = \frac{2(m_\pi + T_\pi)}{\hbar^2} \int V_{\text{opt}}^J(s, s') F^J(s') ds', \quad (61)$$

where  $T_\pi$  is the laboratory bombarding energy,

$$k_0^2 = (T_\pi^2 + 2m_\pi T_\pi)/c^2 \quad (62)$$

and

interaction which is dominant in the resonance region. For ease of calculation we have neglected the Coulomb interaction between the pion and the nucleons.

Most calculations of pion-nucleus scattering use impulse approximation, in which the struck nucleon is treated as effectively free apart from some kinematical corrections. In the impulse approximation one therefore neglects the medium effects due to binding and the exclusion principle.

To see the effects of binding, we compare our results obtained from the three-body model with those obtained from an impulse approximation. Before doing that we briefly discuss the relation between impulse approximation and the three-body model.

The optical potential in modified first order is

$$V_{\text{opt}} = (A - 1) \left[ \Phi_0, \left[ v + v \frac{1}{E - K_\pi - H_T - v + i\epsilon} v \right] \Phi_0 \right], \quad (64)$$

where  $K_\pi$  is the kinetic energy operator of the pion,  $H_T$  is the nuclear Hamiltonian,  $v$  is the  $\pi N$  potential, and  $\Phi_0$  is the target ground state. In the three-body model Eq. (64) becomes

$$V_{\text{opt}} = \frac{A - 1}{A} \sum_n \left[ \psi_n, \left[ v + v \frac{1}{T_\pi + \epsilon_n - K_\pi - K_N - U(r) - v + i\epsilon} v \right] \psi_n \right], \quad (65)$$

where  $\psi_n$  are the occupied single-particle orbitals and  $\epsilon_n$  are the corresponding energies.

The binding potential  $U(r)$  in the optical potential (65) makes the evaluation of  $V_{\text{opt}}$  difficult. In the impulse approximation this potential is omitted and the pion bound-nucleon transition matrix  $t$  is replaced by the pion free-nucleon transition matrix,

$$t_{\text{free}}(\omega) = v + v \frac{1}{\omega - K_\pi - K_N - v + i\epsilon} v, \quad (66)$$

where  $\omega$  is some appropriate  $\pi N$  energy that can be adjusted to approximately represent the missing interaction

with other nucleons. The first order optical potential in the impulse approximation is then

$$V_{\text{opt}}(\omega) = \frac{A-1}{A} \sum_n \left[ \psi_n, \left[ v + v \frac{1}{\omega - K_\pi - K_N - v + i\epsilon} v \right] \psi_n \right] \quad (67)$$

using the same set of occupied orbitals as in Eq. (65). From Eqs. (65) and (67) we see that the essential simplification of the impulse approximation is to replace the binding potential  $U(r)$  by a constant. By this assumption of free nucleon recoil in intermediate states the full effect of the binding of the nucleon on the optical potential is lost.

To continue the discussion of the impulse approximation we rewrite (67) in the form

$$\langle \vec{k}' | V_{\text{opt}} | \vec{k} \rangle = (A-1) \int d\vec{p} d\vec{p}' \langle \vec{k}', \vec{p}' | t_{\text{free}}(\omega) | \vec{k}, \vec{p} \rangle F(\vec{p}', \vec{p}), \quad (68)$$

where  $\vec{k}$  ( $\vec{k}'$ ) and  $\vec{p}$  ( $\vec{p}'$ ) are momenta of the pion and the nucleon in the initial (final) state, respectively, and

$$F(\vec{p}', \vec{p}) = \frac{1}{A} \sum_n \psi_n(\vec{p}') \psi_n(\vec{p}) \quad (69)$$

is the single-nucleon density function. In the simplest impulse approximation  $\omega$  is the physical collision energy of the pion and the nucleon, i.e.,

$$\omega = T_\pi + p_0^2/2M, \quad (70)$$

where  $T_\pi$  is the incident energy of the pion in the pion-nucleus center of mass frame and  $\vec{p}_0$  is the initial momentum of the nucleon in the  $\pi N$  collision. A choice of  $\vec{p}_0$  can be made by assuming that the nucleons are "frozen" in the target nucleus<sup>14</sup> so that each nucleon has a momentum  $\vec{p}_0 = -\vec{k}_0/A$  in the  $\pi A$  center of mass, where  $\vec{k}_0$  is the momentum of the incident pion in the  $\pi A$  center of mass frame. Often  $\omega$  is taken to be a free variable; for example, Landau,<sup>17</sup> Myhrer,<sup>18</sup> and Julius and Rogers<sup>19</sup> choose  $\omega$  to incorporate some binding effects in  $t_{\text{free}}(\omega)$ . They use three-body kinematics for the pion, nucleon, and core to arrive at a value of  $\omega$  (called the three-body energy) which is (assuming an infinitely heavy core)

$$\omega^{3B} = T_\pi + \langle \epsilon_n \rangle, \quad (71)$$

where  $\langle \epsilon_n \rangle$  is the average total energy of a nucleon in the nucleus. The three-body choice of energy can be improved<sup>20</sup> somewhat by replacing the average nucleon energy  $\langle \epsilon_n \rangle$  by the actual energy of the nucleon in the  $n$ th orbital, thereby making  $\omega^{3B}$  dependent on nucleon orbitals

$$\omega_n^{3B} = T_\pi + \epsilon_n. \quad (72)$$

The form (67) or (68) of the optical potential includes nucleon Fermi motion and recoil correctly. Sometimes a further approximation is made by neglecting the dependence of the  $t$  matrix in (68) on the nucleon momenta, i.e., the initial nucleon momentum variable  $\vec{p}$  is replaced by a suitable con-

stant value  $\vec{p}_0$ , as in the previous frozen nucleus approximation. We obtain in this approximation (called the factored or static approximation)

$$\begin{aligned} \langle \vec{k}' | V_{\text{opt}}(\omega) | \vec{k} \rangle \\ = (A-1) \langle \vec{k}', \vec{p}_0 + \vec{q} | t_{\text{free}}(\omega) | \vec{k}, \vec{p}_0 \rangle \rho(\vec{q}), \end{aligned} \quad (73)$$

where  $\vec{q} = \vec{k} - \vec{k}'$  and

$$\rho(\vec{q}) = \int F(\vec{p} + \vec{q}, \vec{p}) d\vec{p}. \quad (74)$$

While the factored approximation is adequate for large nuclei and for pion energies away from the resonance energy, it is inaccurate near resonance.<sup>21</sup> The factored approximation neglects the intermediate propagation of the  $\pi N$  center of mass, i.e., the kinetic energy operator of the  $\pi N$  center of mass is replaced by a constant. Near resonance  $t$  is a rapidly varying function of energy and so the imposition of closure on the  $\pi N$  center of mass leads to large error in the resonance region.

To improve the factored approximation (73) the  $t$  matrix is often Fermi averaged.<sup>14</sup> The Fermi averaging procedures are intuitive prescriptions rather than systematic corrections to a well defined approximation.

We want to investigate the effect of nucleon binding in the scattering of pions from  $^{16}\text{O}$ . So we compare our results from the full three-body calculations with those from the impulse approximation (67), using for  $\omega$  the three-body choice (72) of  $\omega_n^{3B}$ . We note that this choice of  $\omega$  simply implies omission of  $U(r)$  in Eq. (65), leaving the remainder of the three-body calculation of  $V_{\text{opt}}$  unmodified.

#### A. Differential cross section

Figures 7–10 show comparisons of the elastic differential cross sections for  $\pi$ - $^{16}\text{O}$  scattering obtained using the three-body potential (65) and using the optical potential in the impulse approximation [Eq. (67)] with the three-body choice (72) of the  $\pi N$  energy  $\omega$ . These results (and all other results to be

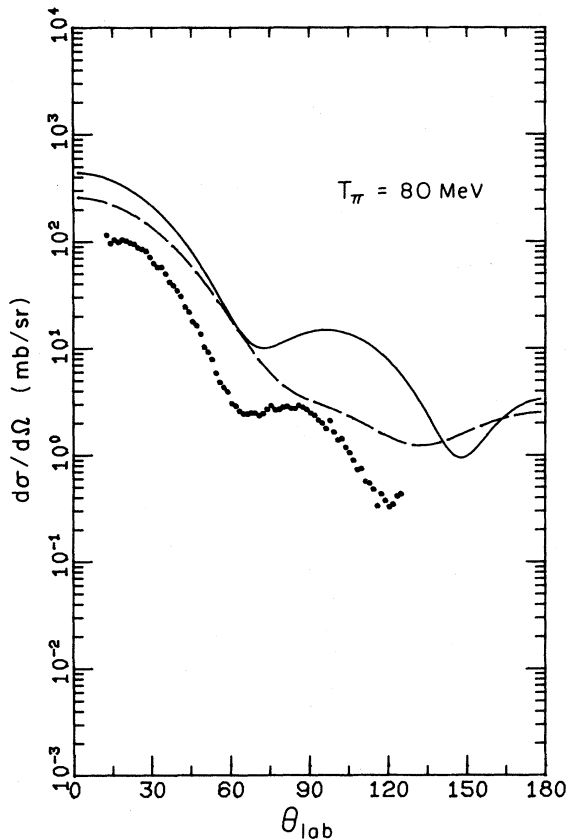


FIG. 7. Differential cross section for  $\pi$ - $^{16}\text{O}$  scattering at laboratory bombarding energy  $T_\pi=80$  MeV. Solid line shows the differential cross section in the three-body model and dashed line shows the differential cross section obtained using the impulse approximation. The dots are experimental points (Ref. 22) for  $\pi^+$ - $^{16}\text{O}$  scattering.

presented subsequently) employ only the  $p$  wave  $\pi N$  interaction and neglect the Coulomb force. For the sake of reference we have also shown with dots the experimental differential cross sections for  $\pi^+$ - $^{16}\text{O}$  scattering,<sup>22</sup> even though our results are not directly comparable with experiment.

We see that the inclusion of the binding potential makes the differential cross section more diffractive for pion energies  $T_\pi < 240$  MeV, indicating an increase in absorption. This may also be inferred from Table I where we show the absolute values of the partial wave scattering matrix  $\eta_J = \exp(2i\delta_J)$  both for the three-body and the impulse approximation calculations. We find that for not too large energies, the  $\eta_J$  are much smaller when binding is included explicitly, i.e., there is more absorption.

The increase in absorption may be understood by examining the nonlocal part of the optical potential. The nonlocal optical potential is complex and it

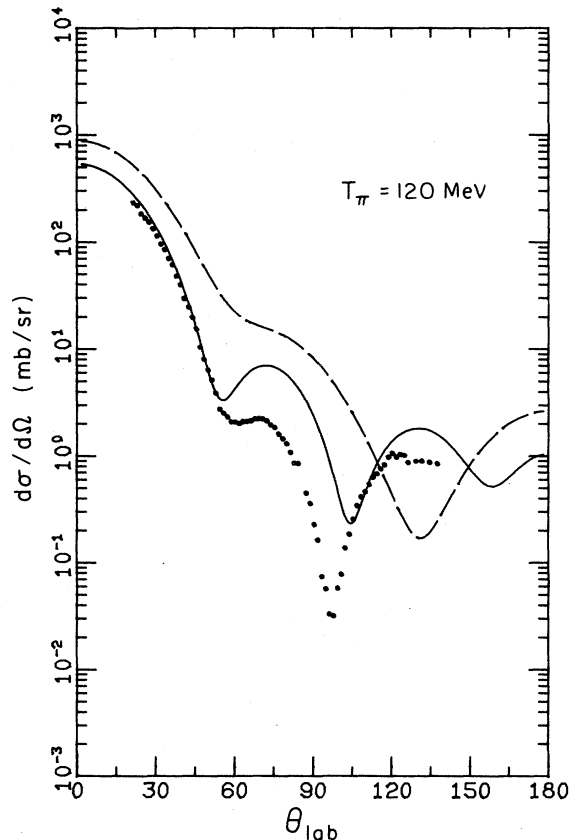


FIG. 8. Differential cross section for  $\pi$ - $^{16}\text{O}$  scattering at laboratory bombarding energy  $T_\pi=120$  MeV. The solid line, the dashed line, and the dots have the same meaning as in Fig. 7.

varies rapidly with energy (because of the  $\pi N$  resonance). We recall that the resonance structure of the nonlocal optical potential is given by the function  $\mathcal{R}(T_\pi + \epsilon_n - \epsilon)$  [see Eqs. (40)–(42)], where  $\epsilon_n$  is the energy of the nucleon in the  $n$ th occupied orbital, and  $\epsilon$  is the excitation energy of the  $\pi N$  center of mass in the intermediate state. In Fig. 11 we plot the real and imaginary parts of  $\mathcal{R}$  as a function of its argument. We notice that  $\text{Im}\mathcal{R}(E)$  attains its maximum value at around 140 MeV, where the  $\text{Re}\mathcal{R}(E)$  passes through zero. Real  $\mathcal{R}(E)$  reaches its maximum value at around 100 MeV, where  $\text{Im}\mathcal{R}(E)$  is reduced to about half its peak value.

The principal difference between impulse approximation and the three-body calculation lies in the range of intermediate state energies  $\epsilon$  that appear in  $\mathcal{R}(T_\pi + \epsilon_n - \epsilon)$ . In the impulse approximation the intermediate states are plane waves and the energies  $\epsilon$  are all positive, with values determined by the free recoil of the struck nucleon. In the three-body calculation, especially at low and moderate pion ener-

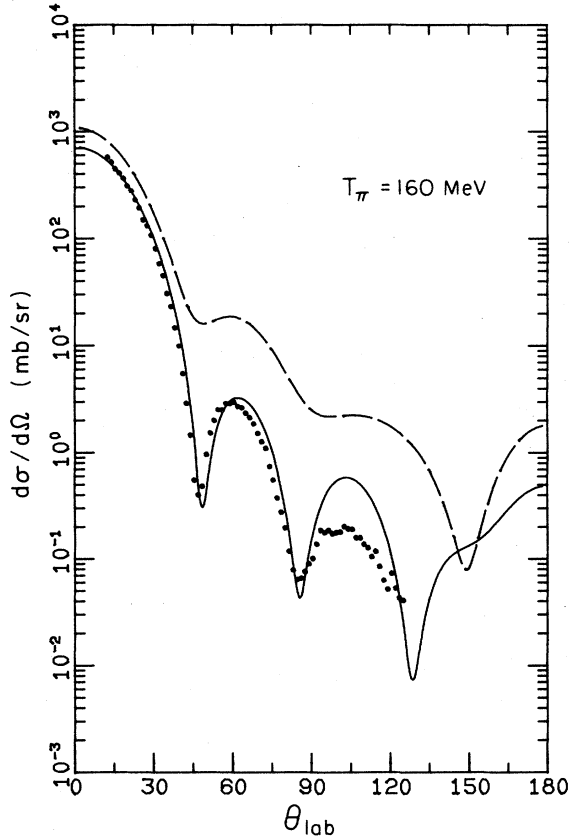


FIG. 9. Differential cross section for  $\pi$ - $^{16}\text{O}$  scattering at laboratory bombarding energy  $T_\pi = 160$  MeV. The solid line, the dashed line, and the dots have the same meaning as in Fig. 7.

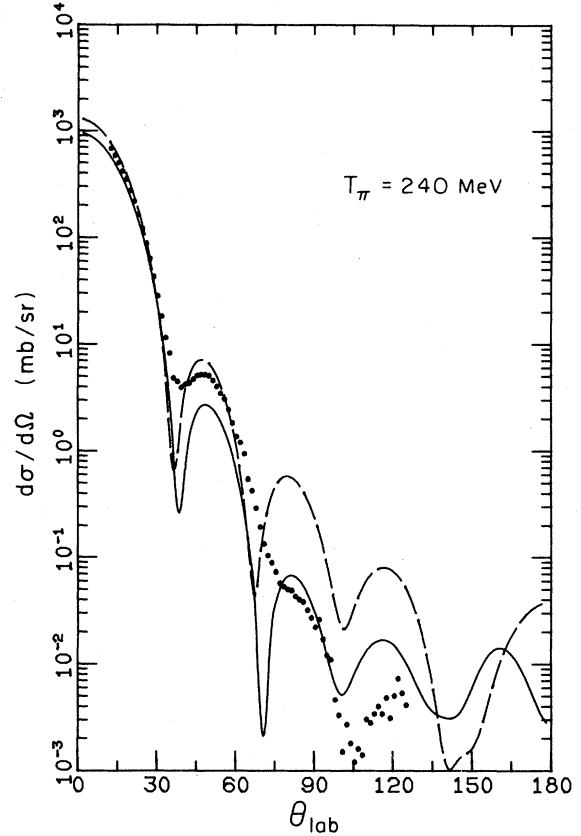


FIG. 10. Differential cross section for  $\pi$ - $^{16}\text{O}$  scattering at laboratory bombarding energy  $T_\pi = 240$  MeV. The solid line, the dashed line, and the dots have the same meaning as in Fig. 7.

gies  $T_\pi$  (as we see later), most of the intermediate excitation goes into bound states and low lying continuum states. As a result, for a given value of  $T_\pi$  the argument of  $\mathcal{R}$  is on the average larger in the three-body calculation than in the impulse calculation. This explains the increased absorption at low to moderate bombarding energies in the three-body calculation, and the other effects seen in Figs. 7–10 and Table I.

It should be noted again that ideal agreement with experiment is not possible in a calculation that omits the Coulomb force, meson annihilation, and  $l=0$  pion-nucleon interactions, and that uses a rather casual spin-independent binding potential  $U(r)$ .

### B. Total cross sections

To investigate further the effects of the binding potential, we plot in Fig. 12 the elastic, reaction, and

total cross sections as functions of the pion bombarding energy  $T_\pi$  in the laboratory frame. The dots are experimental total cross sections, which are taken as the mean of the total cross sections<sup>23</sup> for  $\pi^+$  and  $\pi^-$ .

The most striking result is that at energies below 180 MeV the reaction cross section is increased enormously when the binding potential is included. As noted earlier, this is a consequence of the smaller average excitation energies  $\epsilon$  in the resonance function  $\mathcal{R}$  in the three-body calculation; as a result the pion-nucleon resonance becomes effective at lower bombarding energies.

To represent such effects in the impulse approximation major modifications are required. For example, artificial phenomenological values for the bound state energies  $\epsilon_n$  are sometimes used to compensate for the incorrect excitation energies  $\epsilon$ . Thus, Landau and Thomas<sup>17</sup> used the unphysical value  $\langle \epsilon_n \rangle = -5$  MeV, whereas the average energy of a

TABLE I. Absolute values of the partial wave scattering matrix  $\eta_J = e^{2i\delta_J}$  in three-body and impulse approximation models, for laboratory pion bombarding energies  $T_\pi = 80, 120, 160,$  and  $240$  MeV.

		$T_\pi$				
		$J$	80	120	160	240
Three-body model	0		0.529	0.338	0.244	0.208
	1		0.541	0.092	0.136	0.245
	2		0.549	0.156	0.135	0.261
	3		0.944	0.266	0.269	0.320
	4		0.996	0.827	0.479	0.411
	5		0.999	0.988	0.814	0.561
	6		1.0	0.999	0.968	0.734
	7		1.0	1.0	0.995	0.880
	8		1.0	1.0	0.999	0.961
	9		1.0	1.0	1.0	0.988
Impulse approximation model	0		0.983	0.850	0.436	0.180
	1		1.000	0.773	0.377	0.161
	2		0.981	0.745	0.395	0.135
	3		0.995	0.824	0.270	0.191
	4		0.999	0.967	0.506	0.299
	5		1.0	0.996	0.899	0.406
	6		1.0	0.999	0.982	0.654
	7		1.0	1.0	0.997	0.874
	8		1.0	1.0	0.999	0.963
	9		1.0	1.0	1.0	0.989

nucleon in the ground state of  $^{16}\text{O}$  is about  $-30$  MeV.

### C. Reaction strength

To determine the importance of individual intermediate states we examine the following linear expression for the reaction cross section<sup>24</sup>

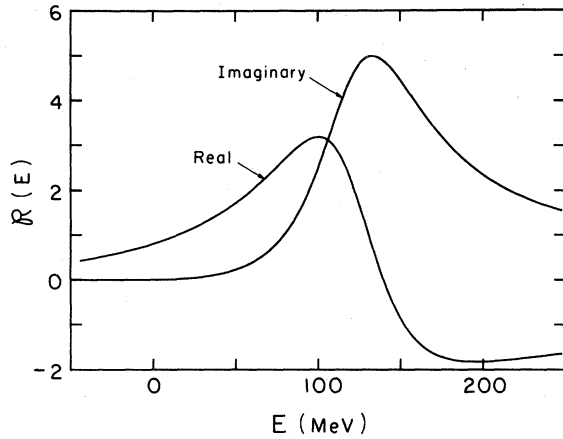


FIG. 11. Real and imaginary parts of the (dimensionless) resonant function  $\mathcal{R}(E)$ .

$$\sigma_R^J = -\frac{2(m_\pi + T_\pi)}{\hbar^2 k^3} 4\pi(2J+1) \times \sum_\epsilon \int ds \operatorname{Im}[F^{J*}(s)V_{\text{opt},\epsilon}^J F^J], \quad (75)$$

where  $F^J(s)$  is the pion wave function for the  $J$ th partial wave and is normalized as

$$F^J(s) \sim \sin(ks - J\pi/2) + ie^{i\delta_J} \sin\delta_J e^{i(ks - J\pi/2)}. \quad (76)$$

Here  $V_{\text{opt},\epsilon}^J$  is the optical potential contribution from an excited state of energy  $\epsilon$ , and  $\sum_\epsilon$  means a sum over the discrete states ( $\epsilon$  negative) and an integral over the continuum excited states ( $\epsilon$  positive).

In Eq. (75) the different  $\epsilon$  values contribute almost independently to  $\sigma_R$ . Thus we may approximately identify the summand in (75) as the differential reaction cross section per unit energy, which we call the reaction strength,

$$\frac{d\sigma_R^J}{d\epsilon} \approx -\frac{2(m_\pi + T_\pi)}{\hbar^2 k^3} 4\pi(2J+1) \times \int ds \operatorname{Im}[F^{J*}(s)V_{\text{opt},\epsilon}^J F^J]. \quad (77)$$

In Figs. 13–16 we show the approximate reaction

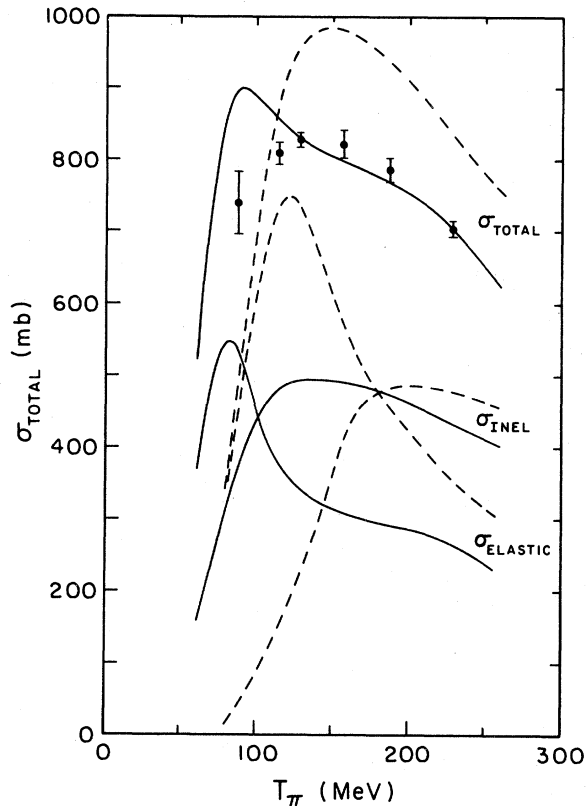


FIG. 12. Total, reaction, and integrated elastic cross sections for  $\pi$ - $^{16}\text{O}$ . The solid lines are the results obtained in the three-body model and the dashed curves are the results obtained in the impulse approximation. Experimental points (Ref. 23) are computed by  $\frac{1}{2}(\sigma_{\pi^+} + \sigma_{\pi^-})$ .

strength for  $J=0, 1, 2, 3, 4,$  and  $5$  at  $T_\pi=160$  MeV as a function of the nucleon excitation energy  $\epsilon$ . The reaction strengths for higher partial waves are negligible at this energy.

For easy comparison of the reaction cross sections from the bound states with those from the continuum states, we plot the contributions of the bound states as vertical bars. For the occupied bound orbitals ( $1s$  and  $1p$ ) with an average energy  $\epsilon=-30$  MeV we draw a bar 5 MeV wide around  $\epsilon=-30$  MeV. We do this for all partial waves, with appropriate heights to represent the reaction cross sections. The reaction cross sections for the excited bound orbitals  $2s$  and  $1d$  (average  $\epsilon=-10$  MeV) are also shown by vertical bars. (Note that excitations to bound states can occur for only  $J \leq 4$ .)

We notice that even at  $T_\pi=160$  MeV, the major contributions to the reaction strengths still come from the bound intermediate states. These introduce strong  $J$  dependent effects in the reaction strengths. Also there are sharp peaks in the reaction strengths near  $\epsilon=1$  MeV and  $\epsilon=5$  MeV. These peaks arise

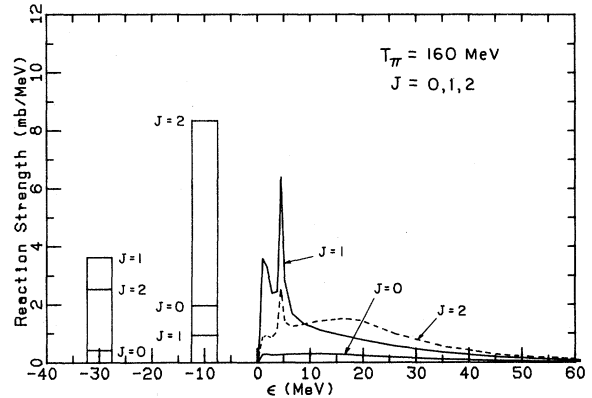


FIG. 13. Contribution of the intermediate states to the reaction strength  $d\sigma_R^J/d\epsilon$  for  $J=0, 1,$  and  $2$  and for laboratory pion energy  $T_\pi=160$  MeV. For continuum excited states with positive energy, the calculated points are joined by straight lines. For the bound excited states ( $2s$  and  $1d$  with a mean energy of about  $-10$  MeV) we draw a bar 5 MeV wide around  $-10$  MeV to represent the contribution to the reaction strength of these states. Similarly the contributions of the occupied bound orbitals ( $1s, 1p$ ) are shown with bars around  $-30$  MeV. The bars for the different partial waves overlap and their heights have to be measured from the horizontal axis.

from the barely unbound  $1f, 2p$  states of the Woods-Saxon potential  $U(r)$ .

For comparison we also show the reaction strengths for impulse approximation (Fig. 17). Here the excited intermediate states are in the continuum and no nuclear structure effects are involved. The reaction strengths are smooth functions of  $\epsilon$ .

Apart from the bound states, low lying continuum states are also emphasized more in the three-body calculation. However, the importance of the bound

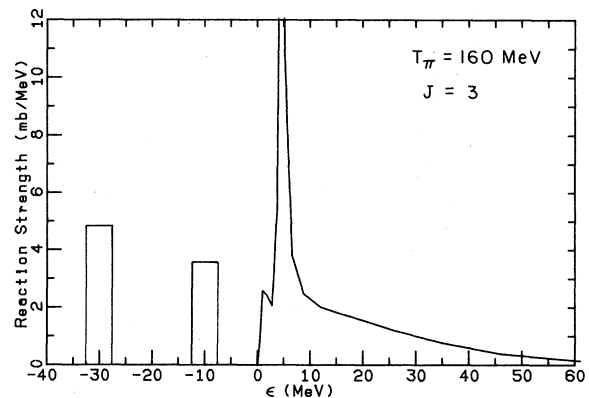


FIG. 14. Reaction strength for  $J=3$  at  $T_\pi=160$  MeV.

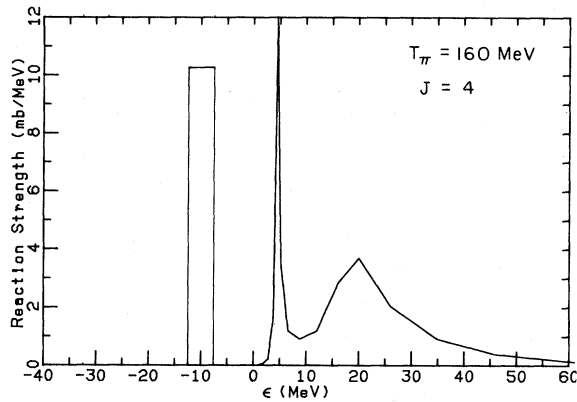


FIG. 15. Reaction strength for  $J=4$  at  $T_\pi=160$  MeV.

states and of the continuum states of low energy decreases as we increase the pion bombarding energy. This is summarized in Table II, where we show the contribution to the reaction cross section from the bound states, from the low energy continuum states ( $\epsilon < 10$  MeV), and from the high energy continuum states ( $\epsilon > 10$  MeV).

From the table we see that for the three-body model the bound states and the low energy continuum states account for nearly 99% of the reaction cross section at  $T_\pi=80$  MeV, whereas at  $T_\pi=240$  MeV they account for about 20% of the reaction cross section. In the impulse approximation model, the low lying states ( $\epsilon < 10$  MeV) account for only 51% of the reaction cross section at  $T_\pi=80$  MeV

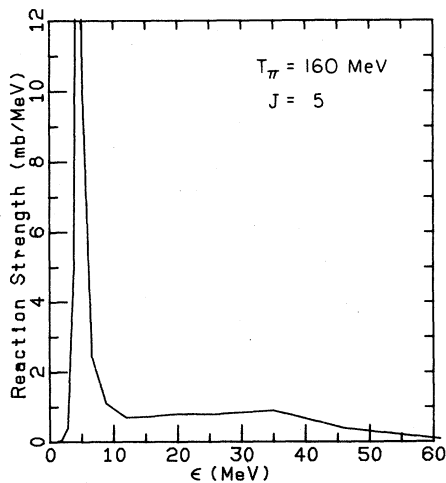


FIG. 16. Reaction strength for  $J=5$  at  $T_\pi=160$  MeV. Note that for  $J=5$  there are no contributions from the bound states. The bound states can only be excited for  $J \leq 4$ .

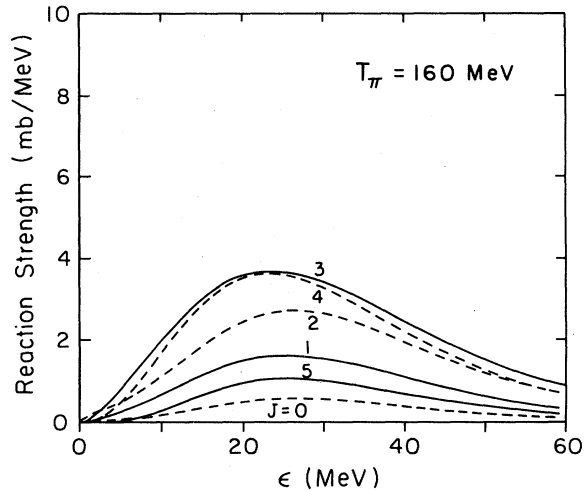


FIG. 17. Contributions of the intermediate states to the reaction strength for  $J=0, 1, 2, 3, 4,$  and  $5$  in the impulse approximation model. Note that in impulse approximations the bound intermediate states are neglected and so the only possible intermediate states are in the continuum with positive energy.

and for 1% of the reaction cross section at  $T_\pi=240$  MeV. Therefore the binding correction to the impulse approximation is substantial at low to moderate energies. Even at  $T_\pi=240$  MeV the binding amounts to about a 20% correction.

Finally, we note from the reaction strength graphs (Figs. 13–16) that states with large excitation energies contribute very little to the reaction cross section. For example, at  $T_\pi=160$  MeV, states with excitation energy  $\epsilon > 30$  MeV are relatively unimportant. Thus the energies of the intermediate states that contribute significantly to the reaction strength are small compared to the pion bombarding energy. This helps justify our neglect of the frame potential term in the optical potential (Sec. IV B). There we found that the frame potential for low lying intermediate states ( $\epsilon \ll T_\pi$ ) is small in magnitude compared to the  $\pi N$  potential and it is quite smooth; hence it can be neglected. However, for large  $\epsilon$  the frame potential is large and oscillatory. Since large  $\epsilon$  values are unimportant, the neglect of the frame potential for all  $\epsilon$  is an appropriate approximation.

#### D. Equivalent local potential

We have used a finite binding potential for the nucleons, unlike other three-body calculations<sup>7,25,26</sup> that are based on a harmonic oscillator binding potential. We therefore have continuum excited states that extend to large radii, and we must expect the derived optical potential to extend beyond the nu-

TABLE II. Reaction cross section (mb) contributions for  $\pi$ - $^{16}\text{O}$  scattering from the bound states, the low lying continuum states ( $\epsilon < 10$  MeV), and high excited ( $\epsilon > 10$  MeV) nucleon states.

		$T^\pi$	80 MeV	160 MeV	240 MeV
Three-body model	$\sigma_R$ (bound)		310.46	192.35	53.08
	$\sigma_R$ ( $\epsilon < 10$ )		12.01	120.67	34.72
	$\sigma_R$ ( $\epsilon > 10$ )		4.26	189.63	340.66
	$\sigma_R$ (bound)/ $\sigma_R$		95%	38.3%	12.4%
	$\sigma_R$ ( $\epsilon < 10$ )/ $\sigma_R$		3.7%	24.0%	8.1%
Impulse approximation model	$\sigma_R$ ( $\epsilon < 10$ )		6.9	19.97	3.03
	$\sigma_R$ ( $\epsilon > 10$ )		6.7	409.55	457.33
	$\sigma_R$ ( $\epsilon < 10$ )/ $\sigma_R$		51%	4.6%	0.7%

clear radius. To investigate these long range effects we calculate the “trivially equivalent local potential” of Perey and Buck,<sup>27</sup> defined by

$$\tilde{V}^J(s) = \frac{\int_0^\infty V_{\text{opt}}^J(s, R) F^J(R) dR}{F^J(s)}, \quad (78)$$

where  $V_{\text{opt}}^J(s, R)$  includes both the local and the non-local parts of the optical potential. This trivially equivalent potential tends to have poles, because the zeroes of the numerator are shifted from those of  $F^J$  in the denominator. But these poles are not important in the surface region.

Our calculations<sup>5</sup> of  $\tilde{V}^J(s)$  show that this rather artificial equivalent potential has appreciable strength ( $\sim 50$  MeV) as much as 1 fm outside the charge radius of  $^{16}\text{O}$ . Such long range interaction effects do not occur in other three-body models of meson scattering.

## VI. SUMMARY AND CONCLUSIONS

We give a calculation of the elastic scattering of mesons by  $^{16}\text{O}$  using a modified first-order KMT multiple scattering theory, in which Pauli blocking effects are omitted from the  $\tau$  operator, as explained in the Introduction and in Sec. II. The modified  $\tau$  operator is calculated in a three-body model, in which each struck nucleon with which the meson interacts is allowed to recoil in the nuclear shell model potential exerted by the remainder of the nucleus.

The three-body model is solved by approximating the shell model potential in excited states as a potential for the meson-nucleon center of mass. This step requires the omission of the difference potential  $U(r_i) - U(R_i)$ , an approximation that is examined at length in Sec. IV B. Matrix elements of the

difference potential are seen to cause weak modifications of the meson optical potential.

The intermediate states of the struck nucleon are found to lie at rather low excitation energies, as one would expect, and are strongly affected by the detailed spectrum of the shell model potential. Bound states and single-particle resonances in the shell-model potential strongly affect the meson scattering. In particular these details of the nuclear spectrum complicate the spectrum of intermediate excited states and enhance the role of low excitation energies. This enhancement of the low-energy intermediate states in turn enhances the scattering at low bombarding energies. It is also interesting that the calculated meson optical potential extends well outside the nuclear surface, presumably related to our use of a Woods-Saxon shell model potential.

Our calculation is primarily a study of the special consequences of a three-body model of the  $\tau$  operator. It does not use any adjustable parameters, and it does not attempt a detailed fit with experiment. Among other limitations of the work reported in the main text are omission of the Coulomb potential, omission of meson annihilation and  $l=0$  meson-nucleon interactions, and the use of a rather casual spin-independent shell model potential. Despite these limitations the calculated cross sections resemble those of experiment. As it happens, since completing this article we were able to repeat the scattering calculations, adding in the  $l=0$  interaction and the Coulomb interaction for  $\pi^+$  mesons. These modifications produce the expected improved agreement with experiment for bombarding energies below 100 MeV. Away from the Coulomb-dominated region the shapes of differential cross sections are not changed very much. At 60 MeV the cross section magnitude is reduced by about a factor of 3; at 80 MeV it is reduced by about 2.

## ACKNOWLEDGMENTS

We are grateful for useful discussions with C. Dover, H. Garcilazo, and W. R. Gibbs, F. Tabakin, and C. M. Vincent. E. Moniz kindly provided infor-

mation about the isobar-doorway work. Numerical data tables for  $\pi^+ - ^{16}\text{O}$  scattering were provided by J. Arvieux. Research support was provided by the National Science Foundation.

- 
- \*Present address: Bio-Imaging Research Inc., 3000 Dundee Road, Suite 320, Northbrook, IL 60062.
- <sup>1</sup>M. Silver and N. Austern, *Phys. Rev. C* **21**, 272 (1980).
- <sup>2</sup>A. K. Kerman, H. McManus, and R. M. Thaler, *Ann. Phys. (N.Y.)* **8**, 551 (1959).
- <sup>3</sup>J. M. Eisenberg and D. S. Koltun, *Theory of Meson Interactions with Nuclei* (Wiley, New York, 1980), pp. 146 and 147.
- <sup>4</sup>P. C. Tandy, E. F. Redish, and D. Bollé, *Phys. Rev. C* **16**, 1924 (1977).
- <sup>5</sup>K. A. Kabir, Ph.D. thesis, University of Pittsburgh, 1982 (unpublished).
- <sup>6</sup>J. Revai, *Nucl. Phys.* **A205**, 20 (1973).
- <sup>7</sup>J. P. Dedonder, *Nucl. Phys.* **A174**, 251 (1971); **A180**, 472 (1972); C. Schmit, *ibid.* **A197**, 449 (1972); J. P. Dedonder and C. Schmit, *Phys. Lett.* **B65**, 131 (1976).
- <sup>8</sup>H. Garcilazo and W. R. Gibbs, *Nucl. Phys.* **A356**, 284 (1981).
- <sup>9</sup>M. Hirata, F. Lenz, and K. Yazaki, *Ann. Phys. (N.Y.)* **108**, 116 (1977); M. Hirata, J. H. Koch, and E. J. Moniz, *ibid.* (N.Y.) **120**, 205 (1979).
- <sup>10</sup>R. A. Freedman, G. A. Miller, and E. M. Henley, *Phys. Lett.* **103B**, 397 (1981).
- <sup>11</sup>J. de Kam, *Phys. Rev. C* **24**, 1554 (1981); E. J. Moniz and A. Sevgen, *ibid.* **C 24**, 224 (1981).
- <sup>12</sup>H. Feshbach, A. Gal, and J. Hüfner, *Ann. Phys. (N.Y.)* **66**, 20 (1971).
- <sup>13</sup>G. E. Brown and W. Weise, *Phys. Rep.* **22C**, 280 (1975); C. Dover and R. H. Lemmer, *Phys. Rev. C* **14**, 2211 (1976).
- <sup>14</sup>R. H. Landau, S. C. Phatak, and F. Tabakin, *Ann. Phys. (N.Y.)* **78**, 299 (1973); S. C. Phatak, F. Tabakin, and R. H. Landau, *Phys. Rev. C* **7**, 1803 (1973); R. H. Landau, *Ann. Phys. (N.Y.)* **92**, 205 (1975).
- <sup>15</sup>M. Silver, Ph.D. thesis, University of Pittsburgh, 1979 (unpublished).
- <sup>16</sup>M. L. Goldberger and K. M. Watson, *Collision Theory* (Wiley, New York, 1974), Sec. 6.8.
- <sup>17</sup>R. H. Landau and A. W. Thomas, *Phys. Lett.* **61B**, 361 (1976).
- <sup>18</sup>F. Myhrer, *Nucl. Phys.* **A241**, 184 (1975).
- <sup>19</sup>D. I. Julius and C. Rogers, *Phys. Rev. C* **12**, 206 (1975).
- <sup>20</sup>E. Kujawski and M. Aitken, *Nucl. Phys.* **A221**, 60 (1974).
- <sup>21</sup>F. Lenz, *Ann. Phys. (N.Y.)* **95**, 348 (1975).
- <sup>22</sup>J. P. Albanese, J. Arvieux, J. Bolger, E. Boschitz, C. H. Q. Ingram, J. Jansen, and J. Zicky, *Nucl. Phys. A* (to be published).
- <sup>23</sup>A. S. Clough, G. K. Turner, B. W. Allardyce, C. J. Batty, D. J. Baugh, W. J. McDonald, R. A. J. Riddle, L. H. Watson, M. E. Cage, G. J. Pyle, and G. T. A. Squier, *Nucl. Phys.* **B76**, 15 (1974).
- <sup>24</sup>John M. Blatt and Victor F. Weisskopf, *Theoretical Nuclear Physics* (Wiley, New York, 1952), Sec. VIII 2a.
- <sup>25</sup>M. G. Piepho and G. E. Walker, *Phys. Rev. C* **9**, 1352 (1974).
- <sup>26</sup>K. K. Bajaj and Y. Nogami, *Phys. Rev. Lett.* **34**, 701 (1975); *Ann. Phys. (N.Y.)* **103**, 141 (1977).
- <sup>27</sup>G. Perey and B. Buck, *Nucl. Phys.* **32**, 353 (1962).